SCIENTIFIC REPORTS

OPEN

Graphene wrapped ordered LiNi$_{0.5}$Mn$_{1.5}$O$_4$ nanorods as promising cathode material for lithium-ion batteries

Xiao Tang[1,2], S. Savut Jan[1,2], Yanyan Qian[1,2], Hui Xia[1,2], Jiangfeng Ni[3], Serguei V. Savilov[4] & Serguei M. Aldoshin[5]

LiNi$_{0.5}$Mn$_{1.5}$O$_4$ nanorods wrapped with graphene nanosheets have been prepared and investigated as high energy and high power cathode material for lithium-ion batteries. The structural characterization by X-ray diffraction, Raman spectroscopy, and Fourier transform infrared spectroscopy indicates the LiNi$_{0.5}$Mn$_{1.5}$O$_4$ nanorods prepared from β-MnO$_2$ nanowires have ordered spinel structure with $P4_332$ space group. The morphological characterization by scanning electron microscopy and transmission electron microscopy reveals that the LiNi$_{0.5}$Mn$_{1.5}$O$_4$ nanorods of 100–200 nm in diameter are well dispersed and wrapped in the graphene nanosheets for the composite. Benefiting from the highly conductive matrix provided by graphene nanosheets and one-dimensional nanostructure of the ordered spinel, the composite electrode exhibits superior rate capability and cycling stability. As a result, the LiNi$_{0.5}$Mn$_{1.5}$O$_4$-graphene composite electrode delivers reversible capacities of 127.6 and 80.8 mAh g^{-1} at 0.1 and 10C, respectively, and shows 94% capacity retention after 200 cycles at 1C, greatly outperforming the bare LiNi$_{0.5}$Mn$_{1.5}$O$_4$ nanorod cathode. The outstanding performance of the LiNi$_{0.5}$Mn$_{1.5}$O$_4$-graphene composite makes it promising as cathode material for developing high energy and high power lithium-ion batteries.

Renewable and sustainable energy resources, such as solar, wind, and tide, attract more and more attention because of the shortage of fossil fuels and their associated environmental problems. However, these renewable energy resources are only intermittently available and require energy storage systems to improve the power reliability and quality[1,2]. Lithium-ion batteries with high energy density, light weight, long cycle life, and environmental friendliness have recently shown potential applications in the areas of electric vehicles and stationary energy storage for smart grids[3]. However, higher requirements are raised by these applications, and further improvements in terms of energy and power densities, safety, and lifetime are imperative for lithium-ion batteries[4].

To further increase the energy density for lithium-ion batteries, various positive electrode materials have been widely investigated to obtain either high working voltage or large capacity. Among them, LiNi$_{0.5}$Mn$_{1.5}$O$_4$ spinel is particularly attractive due to its high average discharge voltage of about 4.7 V (vs. Li/Li$^+$) with a theoretical capacity of about 148 mAh g^{-1}[5,6]. LiNi$_{0.5}$Mn$_{1.5}$O$_4$ can exist in two different crystallographic structures. The disordered LiNi$_{0.5}$Mn$_{1.5}$O$_{4-\delta}$ has the normal face-centered spinel structure

[1]School of Materials Science and Engineering, Nanjing University of Science and Technology, Nanjing 210094, China. [2]Herbert Gleiter Institute of Nanoscience, Nanjing University of Science and Technology, Nanjing 210094, China. [3]College of Physics, Optoelectronics and Energy, Soochow University, Suzhou 215006, China. [4]Department of Chemistry, M. V. Lomonosov Moscow State University, Moscow 119991, Russia. [5]Department of Physical Chemistry Engineering, M. V. Lomonosov Moscow State University, Moscow 119991, Russia. Correspondence and requests for materials should be addressed to H.X. (email: xiahui@njust.edu.cn)
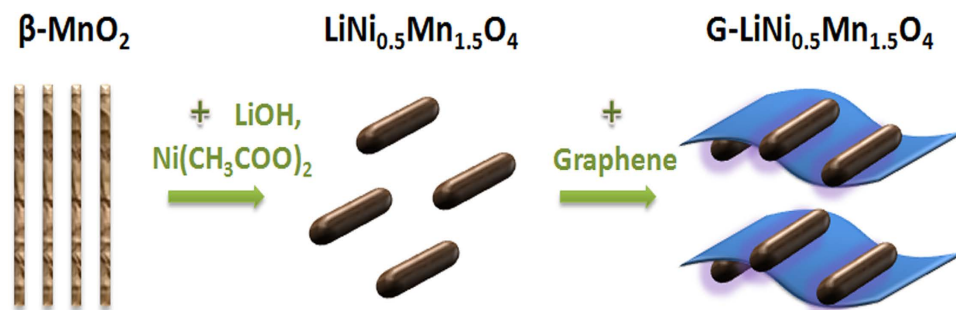
Figure 1. Schematic illustration of the design of the hybrid $LiNi_{0.5}Mn_{1.5}O_4$-graphene electrode material.

with Fd-3m symmetry, while Mn^{4+} and Ni^{2+} ions order in stoichiometric $LiNi_{0.5}Mn_{1.5}O_4$ resulting in the $P4_332$ symmetry[7,8]. The disordered spinel shows higher electronic conductivity due to the presence of Mn^{3+}/Mn^{4+} redox couple and Ni/Mn disordering[9]. However, the nonstoichiometry in disordered spinel often induces impurities such as NiO and Li_xNi_yO, and the 4 V (vs. Li/Li^+) Mn^{3+}/Mn^{4+} redox couple, thus reducing the specific capacity and energy[10]. It is still a challenge to achieve both high energy and high power densities for the ordered spinel due to its poor electronic conductivity. Moreover, the high working voltage at about 4.7 V (vs. Li/Li^+) induces side reactions at the electrode/electrolyte interface, resulting in continuous capacity fading during the cycling[11].

To circumvent the drawbacks of the high voltage spinels, two strategies are often employed to improve the electrochemical performance. One approach is to construct nanostructures for the spinel, which can drastically shorten the transport distance for both electrons and lithium ions, resulting in greatly improved rate capability[12–15]. However, the increased surface area associated with nanostructuring will aggravate the side reactions at high voltage and deteriorate the capacity fading during cycling. Another approach people often used is to modify the spinel surface by coating a thin protective layer, which can greatly improve the interface stability with enhanced cycling performance[16–20]. However, the coating materials, most of which are metal oxides and metal fluorides, only function as protective layers for the spinel without improvement in electrical conductivity. Therefore, new strategies that can combine the advantages of the above mentioned two approaches need to be developed to further improve the electrochemical performance of the high voltage spinels.

Herein, we developed a facile method to prepare graphene nanosheets wrapped ordered $LiNi_{0.5}Mn_{1.5}O_4$ nanorods as high energy and high power cathode material for lithium-ion batteries (Fig. 1). In the hybrid electrode design, the one-dimensional nanostructure of $LiNi_{0.5}Mn_{1.5}O_4$ enables fast lithium ion transport while the graphene wrapping suppresses the side reactions at high voltage and further improves the electron transfer. It has been demonstrated that the graphene or grahene oxide nanosheets incorporation can greatly improve the rate capability and cycling stability for the disordered spinels[21,22]. Consequently, the ordered $LiNi_{0.5}Mn_{1.5}O_4$ nanorods-graphene composite cathode exhibited greatly improved cycling performance and rate performance compared to the bare ordered $LiNi_{0.5}Mn_{1.5}O_4$ nanorods. The promising results indicate the great potential of developing high energy and high power lithium-ion batteries by utilizing the graphene nanosheets wrapped ordered $LiNi_{0.5}Mn_{1.5}O_4$ nanorods.

Results

The hydrothermally prepared β-MnO_2 nanowires were used as the template and the XRD pattern shows no trace of impurity (Fig. S1, Supporting Information). Figure 2 shows the XRD patterns of the pristine graphene nanosheets, the as-synthesized $LiNi_{0.5}Mn_{1.5}O_4$ nanorods, and the $LiNi_{0.5}Mn_{1.5}O_4$-graphene composite. The XRD pattern of the graphene shows a small hump at about 26°, which can be attributed to the (002) reflection of graphite. The as-synthesized $LiNi_{0.5}Mn_{1.5}O_4$ nanorods and the $LiNi_{0.5}Mn_{1.5}O_4$-graphene composite show similar XRD patterns, which can be indexed to the cubic spinel structure with space group $P4_332$ (JCPDS No. 80-2184). No impurity peaks from NiO or Li_xNi_yO can be detected, indicating the existence of pure spinel phase. Rietveld refinement gives a lattice parameter of $a = 8.169$ Å, which agrees well with reported value for the ordered $LiNi_{0.5}Mn_{1.5}O_4$[12,13]. No diffraction peaks of graphene can be observed from the XRD pattern of the $LiNi_{0.5}Mn_{1.5}O_4$-graphene composite, which is probably due to the strong diffraction peaks from the highly crystalline $LiNi_{0.5}Mn_{1.5}O_4$ and the nanoscale size feature of low content graphene. However, the superstructure peaks, which are characteristics of Ni and Mn ordering, cannot be resolved from the XRD patterns of the spinels because of their low intensities[23]. Therefore, further structural investigation by Raman and FTIR are required to confirm the $P4_332$ symmetry of the synthesized spinel in this work.

Raman spectra of the pristine graphene nanosheets, the bare $LiNi_{0.5}Mn_{1.5}O_4$ nanorods, and the $LiNi_{0.5}Mn_{1.5}O_4$-graphene composite are shown in Fig. 3a. The Raman spectra of the bare $LiNi_{0.5}Mn_{1.5}O_4$ nanorods and the $LiNi_{0.5}Mn_{1.5}O_4$-graphene composite show similar features in the frequency range of 300–1000 cm^{-1}, which are in good agreement with published works on ordered $LiNi_{0.5}Mn_{1.5}O_4$ spinel[23,24].
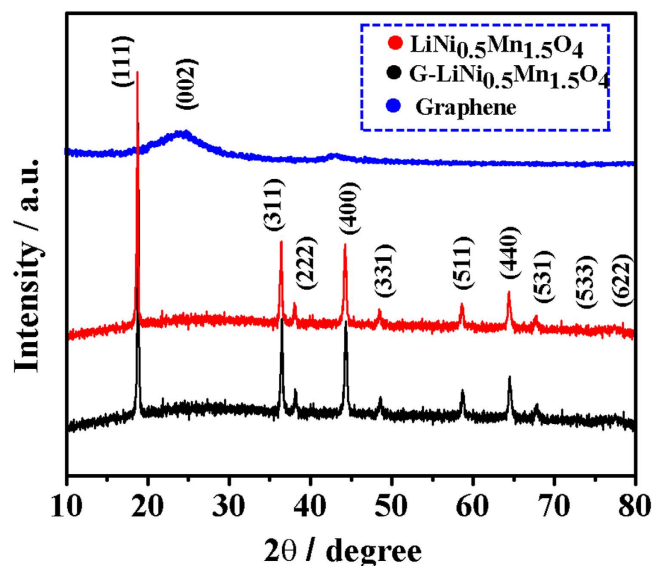
Figure 2. XRD patterns of the pristine graphene nanosheets, the as-synthesized $LiNi_{0.5}Mn_{1.5}O_4$ nanorods, and the $LiNi_{0.5}Mn_{1.5}O_4$-graphene composite.
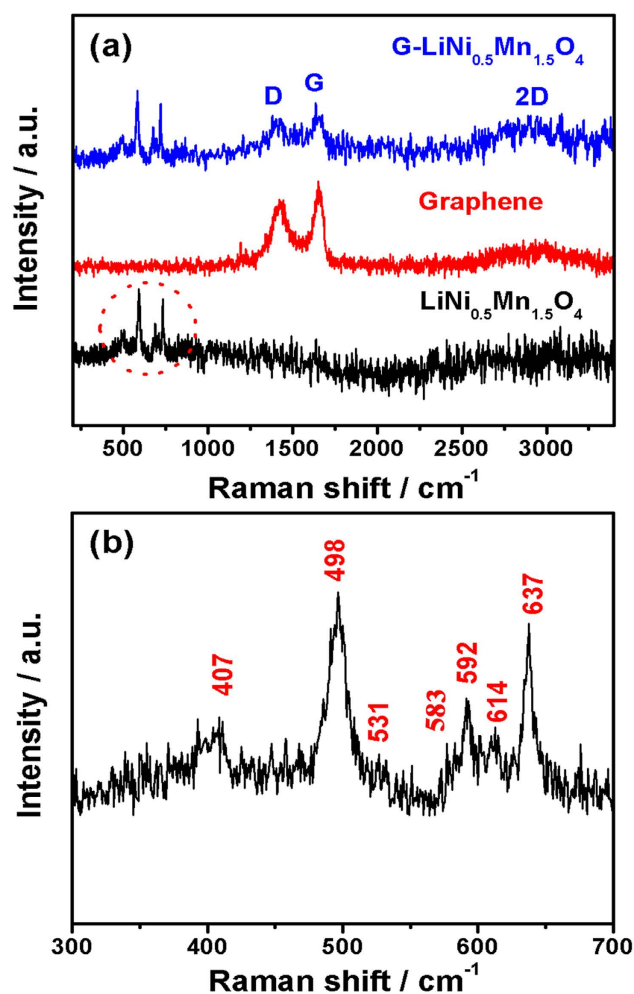

Figure 3. (**a**) Raman spectra of the pristine graphene nanosheets, the bare $LiNi_{0.5}Mn_{1.5}O_4$ nanorods, and the $LiNi_{0.5}Mn_{1.5}O_4$-graphene composite. (**b**) Enlargement of the Raman spectrum of the $LiNi_{0.5}Mn_{1.5}O_4$ nanorods in the frequency range between 300 and 700 cm^{-1}.
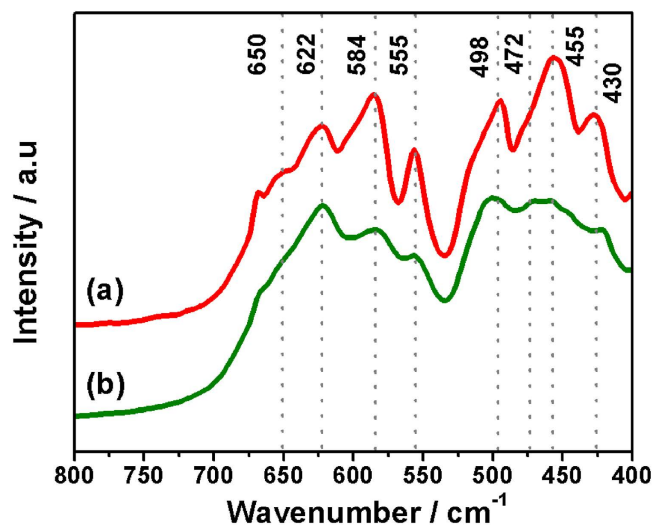
Figure 4. FTIR spectra of (**a**) the ordered LiNi$_{0.5}$Mn$_{1.5}$O$_4$ nanorods and (**b**) the disordered LiNi$_{0.5}$Mn$_{1.5}$O$_4$ powder prepared by a solid state synthesis.

The Raman spectrum of the LiNi$_{0.5}$Mn$_{1.5}$O$_4$ nanorods in the frequency range between 300 to 700 cm^{-1} was enlarged and shown in Fig. 3b, revealing six Raman bands. The strong band around 638 cm^{-1} is assigned to the symmetric Mn-O stretching mode of MnO$_6$ octahedral (A$_{1g}$), while the two bands at 407 and 498 cm^{-1} are associated with the Ni^{2+}-O stretching mode in the structure[25]. The peak near 580–620 cm^{-1} is considered as T2g$^{(3)}$ of the spinel compound, and the split of T2g$^{(3)}$ is the strong evidence of the ordered spinel due to its low symmetry ($P4_332$). In the frequency range between 1000 and 3700 cm^{-1}, the Raman spectrum of the LiNi$_{0.5}$Mn$_{1.5}$O$_4$-graphene composite show similar Raman features as the pristine graphene nanosheets, revealing the characteristic D band, G band, and 2D band of graphene.

To further confirm the structural symmetry of the spinel in the present work, FTIR analysis was carried out on different spinel powder samples. For comparison, disordered LiNi$_{0.5}$Mn$_{1.5}$O$_4$ powders were prepared by a solid state synthesis according to the literature[26]. Figure 4a,b show the FTIR spectra of the as-prepared LiNi$_{0.5}$Mn$_{1.5}$O$_4$ nanorods and the LiNi$_{0.5}$Mn$_{1.5}$O$_4$ powders prepared by solid state synthesis, respectively. There are eight distinctive bands for the as-prepared LiNi$_{0.5}$Mn$_{1.5}$O$_4$ nanorods, and the observed wavenumbers match well with those of ordered spinel in literature[8,23]. By contrast, some bands are not well resolved for the disordered LiNi$_{0.5}$Mn$_{1.5}$O$_4$ because of lacking of Ni/Mn ordering. Another evidence to distinguish the two structures is the change of the intensity ratio of the two bands at 622 and 584 cm^{-1}. In specific, the 584 cm^{-1} Ni-O band increases in intensity compared to the 622 cm^{-1} Mn-O band with increasing level of ordering[8]. Agreeing well with Raman analysis, the FTIR analysis confirms that the as-prepared LiNi$_{0.5}$Mn$_{1.5}$O$_4$ nanorods have ordered spinel structure with $P4_332$ symmetry.

The typical morphologies of β-MnO$_2$ nanowires, LiNi$_{0.5}$Mn$_{1.5}$O$_4$ nanorods, graphene nanosheets, and LiNi$_{0.5}$Mn$_{1.5}$O$_4$-graphene composite are shown in Fig. 5. As shown in Fig. 5a, the β-MnO$_2$ nanowires are about 50–100 nm in diameter and 2-3 μm in length. Figure 5b reveals that the as-synthesized LiNi$_{0.5}$Mn$_{1.5}$O$_4$ nanorods well preserve the one-dimensional morphology of the β-MnO$_2$ nanowires. However, the LiNi$_{0.5}$Mn$_{1.5}$O$_4$ nanorods have larger diameters of about 100–200 nm and shorter lengths of about 0.5–1 μm, which are probably caused by the phase transition and breaking of β-MnO$_2$ nanowires due to the strain associated with the volume expansion. As shown in Fig. 5c, the prepared graphene nanosheets are corrugated and transparent, well resembling the two-dimensional morphology. LiNi$_{0.5}$Mn$_{1.5}$O$_4$-graphene composite shows a laminated morphology (Fig. 5d) with LiNi$_{0.5}$Mn$_{1.5}$O$_4$ nanorods well dispersed on the graphene nanosheets without severe aggregation.

Figure 6a,b show the TEM images of the LiNi$_{0.5}$Mn$_{1.5}$O$_4$ nanorods with low and high magnifications, respectively, revealing the single crystalline feature of the nanorods. The interplanar spacing determined by the HRTEM image in Fig. 6c is about 0.48 nm, which is consistent with the (111) planes of LiNi$_{0.5}$Mn$_{1.5}$O$_4$ spinels. For the LiNi$_{0.5}$Mn$_{1.5}$O$_4$-graphene composite, Fig. 6d,e clearly reveal that the LiNi$_{0.5}$Mn$_{1.5}$O$_4$ nanorods are well distributed and wrapped in the transparent graphene nanosheets. The HRTEM in Fig. 6f shows a clear interface between one LiNi$_{0.5}$Mn$_{1.5}$O$_4$ nanorod and one graphene sheet, indicating good adhesion and close contact between the two components in the composite. The interplanar spacing of about 0.48 nm shown in Fig. 6f is also attributed to the (111) planes of the spinel. The uniform LiNi$_{0.5}$Mn$_{1.5}$O$_4$-graphene heterostructure can be attributed to the facile chemical mixing method. Initially, the mortar grinding can effectively separate the LiNi$_{0.5}$Mn$_{1.5}$O$_4$ nanorods from aggregation. Afterward, the ultrasonication and the continuous stirring facilitate the uniform nanorods distribution in the graphene matrix, resulting the graphene wrapped LiNi$_{0.5}$Mn$_{1.5}$O$_4$ nanorods. The graphene content was determined to be about 4.7 wt% by TGA measurement (Fig. S2, Supporting Information).
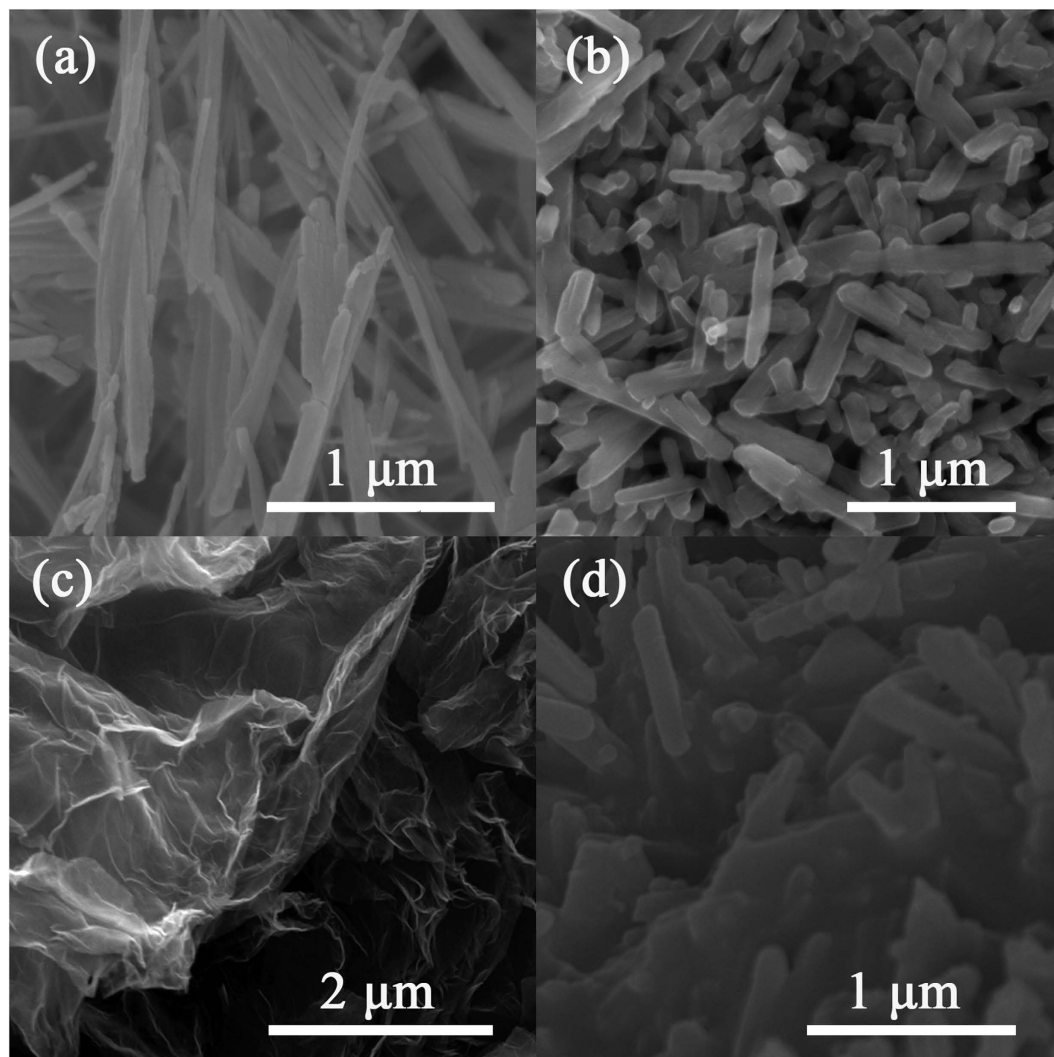
Figure 5. FESEM images of (**a**) the β-MnO_2 nanowires, (**b**) the $LiNi_{0.5}Mn_{1.5}O_4$ nanorods, (**c**) the pristine graphene nanosheets, and (**d**) the $LiNi_{0.5}Mn_{1.5}O_4$-graphene composite.

To evaluate the electrochemical properties of the $LiNi_{0.5}Mn_{1.5}O_4$-graphene composite, half cells were assembled using lithium foil as both counter and reference electrodes. Fig. 7 compares the typical CV curves of the bare $LiNi_{0.5}Mn_{1.5}O_4$ nanorod electrode and the $LiNi_{0.5}Mn_{1.5}O_4$-graphene composite electrode between 3.5 and 5 V (vs. Li/Li$^+$) at a scan rate of 0.05 mV s^{-1}. For both electrodes, a pair of strong redox peaks at about 4.7 V (vs. Li/Li$^+$) can be clearly observed, which can be attributed to the Ni^{2+}/Ni^{4+} redox reactions[8,27]. The 4 V redox peaks, corresponding to the Mn^{3+}/Mn^{4+} redox couple, are almost negligible in the CV curves for the bare $LiNi_{0.5}Mn_{1.5}O_4$ nanorod electrode and the $LiNi_{0.5}Mn_{1.5}O_4$-graphene composite electrode, indicating their nearly perfect stoichiometry. By contrast, apart from the obvious 4 V (vs. Li/Li$^+$) redox peaks, the disordered $LiNi_{0.5}Mn_{1.5}O_4$ will show clear two pairs of redox peaks at about 4.7 V (vs. Li/Li$^+$) in CV[28]. Previous studies indicate that the redox peak splitting at about 4.7 V (vs. Li/Li$^+$) for the high voltage $Li_xNi_{0.5}Mn_{1.5}O_4$ (0 < x < 1) is probably due to two separate redox couples of Ni^{2+}/Ni^{3+} and Ni^{3+}/Ni^{4+} and/or Li/vacancy ordering at x = 0.5[29]. However, such peak splitting is not obvious for the ordered spinel as only one pair of redox peaks are observed in the typical CV curve. As discussed in our previous work on disordered $LiNi_{0.5}Mn_{1.5}O_{4-\delta}$ thin films[30], the ordering arrangement of Ni and Mn in the ordered spinel is probably not commensurate with the preferred Li/vacancy ordering at x = 0.5 so that the Ni/Mn ordering suppresses Li/vacancy ordering and redox peak splitting at about 4.7 V (vs. Li/Li$^+$). In comparison with the bare $LiNi_{0.5}Mn_{1.5}O_4$ nanorod electrode, the $LiNi_{0.5}Mn_{1.5}O_4$-graphene composite electrode shows much smaller peak separation between the cationic peak and anodic peak in the CV curve, indicating the electrode polarization can be greatly reduced by incorporating the graphene nanosheets into $LiNi_{0.5}Mn_{1.5}O_4$ nanorods.

Figure 8a,b show the charge/discharge curves of the bare $LiNi_{0.5}Mn_{1.5}O_4$ nanorod and the $LiNi_{0.5}Mn_{1.5}O_4$-graphene composite electrodes, respectively, at the 1st, 2nd, 50th, 100th, and 200th cycles at a current rate of 0.1 C between 3.0 and 4.9 V (vs. Li/Li$^+$). Agreeing well with the CV results, the
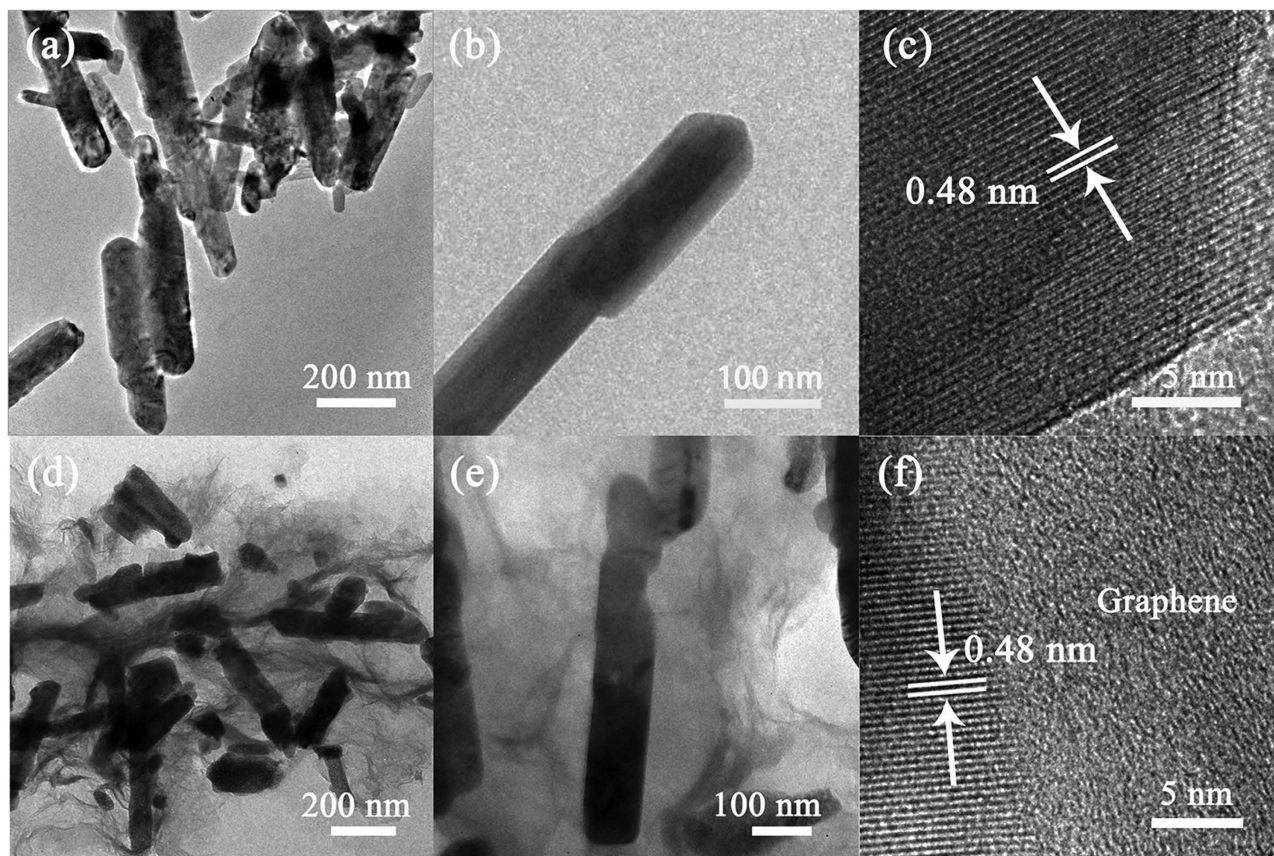
Figure 6. (**a–c**) TEM and HRTEM images of the bare $LiNi_{0.5}Mn_{1.5}O_4$ nanorods. (**d–f**) TEM and HRTEM images of the $LiNi_{0.5}Mn_{1.5}O_4$-graphene composite.
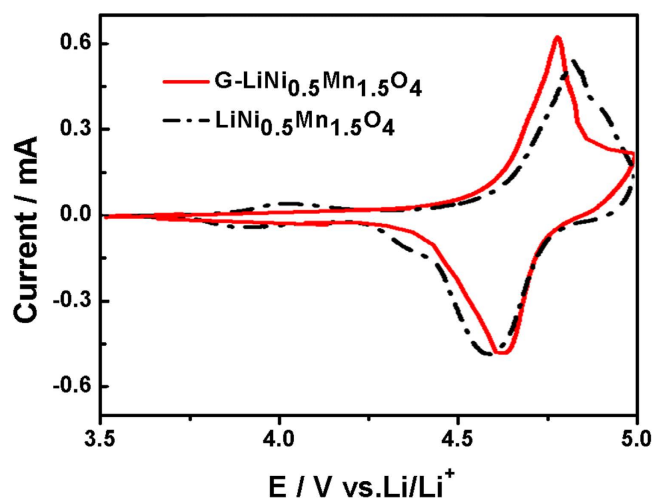
Figure 7. Typical CV curves of the bare $LiNi_{0.5}Mn_{1.5}O_4$ nanorod electrode and the $LiNi_{0.5}Mn_{1.5}O_4$-graphene composite electrode.

charge/discharge curves of the two electrodes clearly show only one flat voltage plateau around $4.70\,V$ (vs. Li/Li^+) due to the Ni^{2+}/Ni^{4+} redox couple, which is the characteristic electrochemical behavior of the ordered spinel[8]. In comparison, the charge/discharge curves of the $LiNi_{0.5}Mn_{1.5}O_4$-graphene composite electrode show much smaller voltage difference between charge and discharge voltage plateaus, indicating smaller polarization and internal resistance of the spinel electrode with graphene incorporation. The first charge and discharge capacities of the $LiNi_{0.5}Mn_{1.5}O_4$-graphene composite electrode are 127.6 and $122.4\,mAh\,g^{-1}$, with a coulombic efficiency of about 96%. By contrast, the first charge and
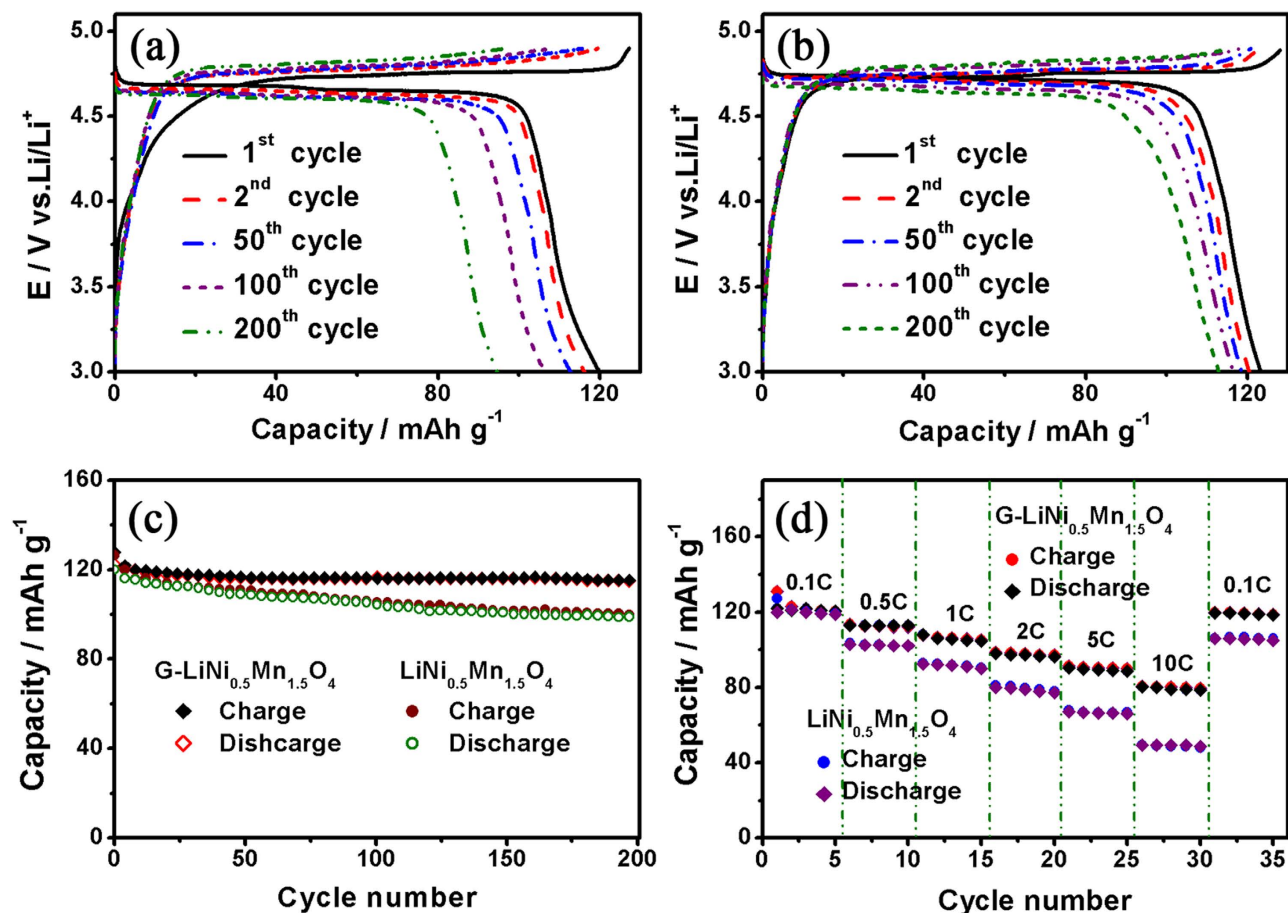
Figure 8. (**a**) Charge/discharge curves of the bare $LiNi_{0.5}Mn_{1.5}O_4$ nanorod electrode at various cycle numbers at 0.1 C rate. (**b**) Charge/discharge curves of the $LiNi_{0.5}Mn_{1.5}O_4$-graphene composite electrode at various cycle numbers at 0.1 C rate. (**c**) Comparison of cycle performance between the bare $LiNi_{0.5}Mn_{1.5}O_4$ nanorod electrode and the $LiNi_{0.5}Mn_{1.5}O_4$-graphene composite electrode. (**d**) Comparison of rate capability between the bare $LiNi_{0.5}Mn_{1.5}O_4$ nanorod electrode and the $LiNi_{0.5}Mn_{1.5}O_4$-graphene composite electrode.

discharge capacities of the bare $LiNi_{0.5}Mn_{1.5}O_4$ nanorod electrode are 127.3 and 119.7 mAh g^{-1}, respectively, with a coulombic efficiency of about 94%. It is clear that the $LiNi_{0.5}Mn_{1.5}O_4$-graphene composite electrode can deliver a larger reversible capacity and higher coulombic efficiency compared to the bare $LiNi_{0.5}Mn_{1.5}O_4$ nanorod electrode. The larger reversible capacity of the $LiNi_{0.5}Mn_{1.5}O_4$-graphene composite electrode can be attributed to the smaller polarization of the electrode, which favors fast charge transport and increases the utilization of the active material. The initial irreversible capacity loss is partially contributed by the solid electrolyte interface (SEI) layer formation due to the electrolyte decomposition at high voltage[31]. The wrapping with graphene could greatly suppress the SEI layer formation at high voltage, thus improving the initial coulombic efficiency of the composite electrode. Figure 8c compares the cycle performance of the two electrodes, revealing greatly improved cycling stability for the $LiNi_{0.5}Mn_{1.5}O_4$-graphene composite electrode. After 200 cycles at 0.1 C rate, $LiNi_{0.5}Mn_{1.5}O_4$-graphene composite electrode can still deliver a reversible capacity of about 115 mAh g^{-1}, retaining 94% of its initial reversible capacity. In comparison, the bare $LiNi_{0.5}Mn_{1.5}O_4$ nanorod electrode only retained 82% of its initial reversible capacity. The capacity fading of the high voltage spinel during cycling is mainly contributed by the structural deterioration induced by Mn^{3+} ion dissolution and internal resistance increase induced by the side reactions at the electrode surface at high voltage[32,33]. For the ordered spinel, Mn^{3+} ion dissolution may not be the major reason that causes the capacity fading since there are negligible Mn^{3+} ions in ordered spinel due to its nearly perfect stoichiometry. The side reactions, including SEI layer formation, could be more detrimental to the cycle performance because the increased polarization induced by the increasing resistance will lead to less reversible capacity. As shown in Fig. 8a, the voltage difference between charge and discharge keeps increasing with the cycling test, revealing a obvious cell polarization growth for the bare $LiNi_{0.5}Mn_{1.5}O_4$ nanorod electrode. By contrast, the polarization growth for the $LiNi_{0.5}Mn_{1.5}O_4$-graphene composite electrode is greatly mitigated, which can be attributed to the graphene protection, suppressing the side reactions at the electrode surface. Figure 8d compares the rate capability of the two electrodes by plotting the specific capacity as a function of cycle number

at different current rates. The typical charge/discharge curves of bare $LiNi_{0.5}Mn_{1.5}O_4$ nanorod electrode and the $LiNi_{0.5}Mn_{1.5}O_4$-graphene composite electrode at different current rates are shown in Fig. S3 (Supporting Information). It is obvious that the $LiNi_{0.5}Mn_{1.5}O_4$-graphene composite electrode possesses much better rate capability as it can retain more reversible capacity as the discharge rate increases. Even at 10 C rate, the $LiNi_{0.5}Mn_{1.5}O_4$-graphene composite electrode can still deliver a reversible capacity of about $80.8\,mAh\,g^{-1}$, which is much larger than that of the bare $LiNi_{0.5}Mn_{1.5}O_4$ nanorod electrode ($49.2\,mAh\,g^{-1}$). When the current rate was set back to 0.1 C, the charge and discharge capacities of $LiNi_{0.5}Mn_{1.5}O_4$-graphene composite electrode recover to the original values, indicating that large current density and rapid lithiation/delithiation did not cause any permanent damage to the crystal structure. However, after the bare $LiNi_{0.5}Mn_{1.5}O_4$ nanorod electrode experienced the high current rate like 10 C, its reversible capacity didn't fully recover to the initial value when the current rate was changed back to 0.1 C. The superior rate performance of the $LiNi_{0.5}Mn_{1.5}O_4$-graphene composite electrode can be attributed to the improved electron transport provided by the graphene conductive matrix. As confirmed by the EIS measurements, the $LiNi_{0.5}Mn_{1.5}O_4$-graphene composite electrode shows much smaller charge transfer resistance compared to the bare $LiNi_{0.5}Mn_{1.5}O_4$ nanorod electrode, indicating the graphene wrapping is beneficial to fast electrode kinetics (Fig. S4, Supporting Information).

Discussion

Although the conductivity of the ordered $LiNi_{0.5}Mn_{1.5}O_4$ is relatively low, the ordered $LiNi_{0.5}Mn_{1.5}O_4$ nanorod-graphene composite developed in this work exhibited excellent rate capacity as well as good cycling stability. The rate performance of the present ordered $LiNi_{0.5}Mn_{1.5}O_4$-graphene composite is even better than those of the previously reported disordered $LiNi_{0.5}Mn_{1.5}O_4$-grahene composite and disordered $LiNi_{0.5}Mn_{1.5}O_4$-grahene oxide composite[21,22], which can be attributed to its unique hybrid electrode design. First, the one-dimensional nanostructure of ordered $LiNi_{0.5}Mn_{1.5}O_4$ provides short solid diffusion length for lithium ions. This, along with fast electron transport supplied by the highly conductive graphene matrix, endows the hybrid electrode with fast lithiation and delithiation capability. Second, the ordered $LiNi_{0.5}Mn_{1.5}O_4$ nanorods with $P4_332$ symmetry contain negligible Mn^{3+} ions, which minimizes Mn disproportionative dissolution and Jahn-Teller structural distortion, resulting in good structural stability during cycling. Last, the graphene wrapping effectively modify the surface of $LiNi_{0.5}Mn_{1.5}O_4$, which suppresses the side reactions at the electrode/electrolyte interface, resulting in a slow cell polarization growth and excellent cycling stability. Unlike disordered $LiNi_{0.5}Mn_{1.5}O_4$, the ordered $LiNi_{0.5}Mn_{1.5}O_4$ do not have the 4 V voltage plateau, thus making the $LiNi_{0.5}Mn_{1.5}O_4$-grpahene composite more promising for application in high energy and high power lithium-ion batteries.

In summary, a smart hybrid cathode material featuring graphene nanosheets wrapped one-dimensional ordered $LiNi_{0.5}Mn_{1.5}O_4$ nanorods has been developed by a facile method combining oxide template synthesis and chemical mixing. The structural characterization confirmed the as-prepared $LiNi_{0.5}Mn_{1.5}O_4$ nanorods possess a ordered spinel structure with $P4_332$ symmetry. The $LiNi_{0.5}Mn_{1.5}O_4$-graphene composite electrode exhibited excellent rate capability, delivering reversible capacities of 122.4 and $81.2\,mAh\,g^{-1}$ at 0.1 and 10 C, respectively. In addition to the fast charge and discharge capability, the $LiNi_{0.5}Mn_{1.5}O_4$-graphene composite electrode also revealed promising cycling stability, with 94% capacity retained after 200 cycles. In comparison with the bare $LiNi_{0.5}Mn_{1.5}O_4$ nanorod electrode, the composite electrode showed greatly improved electrochemical performance, which can be ascribed to the smart hybrid electrode design, enabling both fast charge transport and good interface stability. The superior electrochemical performance and the facile synthesis procedure make the present $LiNi_{0.5}Mn_{1.5}O_4$-graphene composite promising as cathode for high energy lithium-ion batteries.

Methods

Preparation β-MnO₂ nanowires and ordered $LiNi_{0.5}Mn_{1.5}O_4$ nanorods. β-MnO_2 nanowires were prepared by a modified hydrothermal method according to the literature[34]. In a typical synthesis, 10 g KNO_3 were added into a solution containing 20 ml 50 wt% $MnNO_3$ and 20 ml deionized water to get a supersaturated system. Then the well mixed solution was transferred into a 50 mL Teflon-lined stainless steel autoclave and heated at 140 °C for 14 h. After cooling down to room temperature, the precipitated product was filtered and washed sequentially with deionized water and ethanol for three times. The obtained β-MnO_2 nanowires were then dried at 80 °C for 6 h in air for further usage. The ordered spinel $LiNi_{0.5}Mn_{1.5}O_4$ nanorods were then synthesized by using the β-MnO_2 nanowires as the template. Briefly, stoichiometric amounts of $Ni(CH_3COO)_2$, $LiOH \cdot H_2O$, and β-MnO_2 nanowires were homogeneously dispersed in high purity ethanol and stirred for 24 h. The obtained precursor was dried at 60 °C for 3 h and ground in a mortar for 1 h. After that, the mixture was first preheated at 300 °C for 5 h and then calcined at 700 °C for 10 h in air to obtain the ordered $LiNi_{0.5}Mn_{1.5}O_4$ nanorods.

Preparation of $LiNi_{0.5}Mn_{1.5}O_4$-graphene composite. The grapnehe nanosheets were prepared from graphite powder in a two-step process, involving the oxidation and/or exfoliation of graphite to graphite oxide by Hummer's method and chemical reduction of graphite oxide to graphene according to literature[35]. To prepare the graphene wrapped $LiNi_{0.5}Mn_{1.5}O_4$ nanorods, 0.05 g graphene and 1 g $LiNi_{0.5}Mn_{1.5}O_4$ nanorods were first mixed in a mortar for 0.5 h by grinding, and then dispersed in 30 ml ethanol by ultrasonication. After that, the dispersion was vigorously stirred at 50 °C for 8 h to achieve a

uniform dispersion of $LiNi_{0.5}Mn_{1.5}O_4$ nanorods in the graphene matrix. Finally, the obtained mixture was dried in an oven at 80 °C overnight to obtain $LiNi_{0.5}Mn_{1.5}O_4$-graphene composite.

Materials Characterization. Structural features of the as-prepared $LiNi_{0.5}Mn_{1.5}O_4$ nanorods and the $LiNi_{0.5}Mn_{1.5}O_4$-graphene composite were characterized with X-ray diffraction (XRD), Raman spectroscopy, and Fourier transform infrared (FTIR) spectroscopy. The XRD patterns were taken by a Shimadzu XRD-6000 X-ray diffractormeter with Cu Kα radiation between 10 and 80°. Raman spectra of different samples were acquired using a Renishaw in Via Reflex Raman microprobe with a 532 nm wavelength incident laser. FTIR spectra of the samples were collected from 800 to 400 cm^{-1} using a Nicolet-670 FTIR spectrometer. To determine the graphene content in the composite, thermogravimetric analysis (TGA) was carried out in the air at a heating rate of 10 °C min^{-1} from 30 to 700 °C using a DTG-60H Shimadzu thermal analyzer. The morphology features of the as-prepared samples were characterized with field-emission scanning electron microscopy (FESEM, JSM-6700F 15 kV), transmission electron microscopy (TEM) and high-resolution transmission electron microscopy (HRTEM, JEOL 2010 200 kV).

Electrochemical Measurements. To investigate the electrochemical properties, half cells using lithium foil as both counter and reference electrodes were assembled with Lab-made Swagelok cells in an Ar-filled glove box. To prepare the working electrodes, active cathode materials ($LiNi_{0.5}Mn_{1.5}O_4$ nanorods and $LiNi_{0.5}Mn_{1.5}O_4$-graphene composite), acetylene black (Super-P) and polyvinylidene fluoride (PVDF) with a weight ratio of 8:1:1 were mixed with N-methyl-2-pyrrolidinone (NMP) to form a slurry. The obtained slurry was coated onto the Al foils and dried at 120 °C for 2 h to remove the solvent. The electrodes were then pressed and cut into small disks (10 mm in diameter). The small disks were further dried at 80 °C in a vacuum oven for 12 h before battery tests. 1 M LiPF$_6$ in ethylene carbonate and diethyl carbonate (EC/DEC, v/v = 1:1) solution was used as the electrolyte and Celgard 2400 membrane was used as the separator. The galvanostatic charge/discharge measurements were carried out on a LAND CT2001A electrochemical workstation with a voltage window between 3.0 and 4.9 V (vs. Li$^+$/ Li) at different current densities (1 C is 148 mAh g^{-1} for $LiNi_{0.5}Mn_{1.5}O_4$) at room temperature. Cyclic voltammogram (CV) and electrochemical impedance spectroscopy (EIS) measurements were performed using a CHI660D electrochemical workstation. CVs were measured between 3.5 and 5.0 V (vs. Li/Li$^+$) at a scan rate of 0.05 mV s^{-1}. EIS measurements were carried out in the frequency range between 100 kHz to 0.01 Hz with an AC amplitude of 5 mV at an open circuit potential.

References

1. Reddy, M. V., Subba Rao, G. V. & Chowdari, B. V. R. Metal Oxides and Oxysalts as anode materials for Li ion batteries. *Chem. Rev.* **113,** 5364–5457 (2013).
2. Cheng, F. Y., Liang, J., Tao, Z. L. & Chen, J. Functional materials for rechargeable batteries. *Adv. Mater.* **23,** 1695–1715 (2011).
3. Xu, B., Qian, D., Wang, Z. Y. & Meng, Y. S. Recent progress in cathode materials research for advanced lithium ion batteries. *Mater. Sci. Eng. R* **73,** 51–65 (2012).
4. Kim, H. *et al.* Aqueous rechargeable Li and Na batteries. *Chem. Rev.* **114,** 11788–11827 (2014).
5. Wang, G. *et al.* Submicron lithium nickel manganese oxide spinel with long cycling stability and high rate performance prepared by a facile route. *J. Power Sources* **265,** 118–124 (2014).
6. Wang, H. L., Tan, T. A., Yang, P., Lai, M. O. & Lu, L. High-rate performances of the Ru-doped spinel $LiNi_{0.5}Mn_{1.5}O_4$: effects of doping and particle size. *J. Phys. Chem. C* **115,** 6102–6110 (2011).
7. Ariyoshi, K., Iwakoshi, Y., Nakayama, N. & Ohzuku, T. Topotactic two-phase reaction of Li[Ni$_{1/2}$Mn$_{3/2}$]O4 (*P*4$_3$32) in nonaqueous lithium cells. *J. Electrochem. Soc.* **151,** A296–A303 (2004).
8. Kunduraci, M. & Amatucci, G. G. Synthesis and characterization of nanostructured 4.7 V Li$_x$Mn$_{1.5}$N$_{i0.5}$O$_4$ spinels for high-power lithium-ion batteries. *J. Electrochem. Soc.* **153,** A1345–A1352 (2006).
9. Lee, H. W., Muralidharan, P., Mari, C. M., Ruffo, R. & Kim, D. K. Facile synthesis and electrochemical performance of ordered $LiNi_{0.5}Mn_{1.5}O_4$ nanorods as a high power positive electrode for rechargeable Li-ion batteries. *J. Power Sources* **196,** 10712–10716 (2011).
10. Xia, H., Tang, S. B., Lu, L., Meng, Y. S. & Ceder, G. The influence of preparation conditions on electrochemical properties of $LiNi_{0.5}Mn_{1.5}O_4$ thin film electrodes by PLD. *Electrochim. Acta* **52,** 2822–2828 (2007).
11. Song, J. *et al.* Role of oxygen vacancies on the performance of Li[Ni$_{0.5-x}$Mn$_{1.5+x}$]O$_4$ (x = 0, 0.05, and 0.08) spinel cathodes for lithium-ion batteries. *Chem. Mater.* **24,** 3101–3109 (2012).
12. Yang, J., Zhang, X., Zhu, Z., Cheng, F. & Chen, J. Ordered spinel $LiNi_{0.5}Mn_{1.5}O_4$ nanorods for high-rate lithium-ion batteries. *J. Electroanaly. Chem.* **688,** 113–117 (2013).
13. Zhang, X., Cheng, F., Yang, J. & Chen, J. $LiNi_{0.5}Mn_{1.5}O_4$ porous nanorods as high-rate and long-life cathodes for Li-ion batteries. *Nano Lett.* **13,** 2822–2825 (2013).
14. Chen, Z. *et al.* Surface-oriented and nanoflake-stacked $LiNi_{0.5}Mn_{1.5}O_4$ spinel for high-rate and long-cycle-life lithium ion batteries. *J. Mater. Chem.* **22,** 17768–17772 (2012).
15. Ding, Y. L., Goh, B. M., Zhang, H., Loh, K. P. & Lu, L. Single-crystalline nanotubes of spinel lithium nickel manganese oxide with lithium titanate anode for high-rate lithium ion batteries. *J. Power Sources* **236,** 1–9 (2013).
16. Zhou, L., Zhao, D. Y. & Lou, X. W. $LiNi_{0.5}Mn_{1.5}O_4$ hollow structures as high-performance cathodes for lithium-ion batteries. *Angew. Chem. Inter. Ed.* **51,** 239–241 (2012).
17. Gao, X. W. *et al.* Improving the electrochemical performance of the $LiNi_{0.5}Mn_{1.5}O_4$ sinel by polypyrrole coating as a cathode material for the lithium-ion battery. *J. Mater. Chem. A* **3,** 404–411 (2015).
18. Konishi, H. *et al.* Effect of surface Li$_3$PO$_4$ coating on $LiNi_{0.5}Mn_{1.5}O_4$ epitaxial thin film electrodes synthesized by pulsed laser deposition. *J. Power Sources* **269,** 293–298 (2014).
19. Kim, K., Kim, Y., Oh, E. S. & Shin, H. C. The role of fluoride in protecting $LiNi_{0.5}Mn_{1.5}O_4$ electrodes against high temperature degradation. *Electrochim. Acta* **114,** 387–393 (2013).
20. Deng, H. F. *et al.* Highly enhanced lithium storage capability of $LiNi_{0.5}Mn_{1.5}O_4$ by coating with Li$_2$TiO$_3$ for Li-ion batteries. *J. Mater. Chem. A* **2,** 18256–18262 (2014).

21. Richard Prabakar, S. J., Hwang, Y. H., Lee, B., Sohn, K. S. & Pyo, M. Graphene-sandwiched LiNi$_{0.5}$Mn$_{1.5}$O$_4$ cathode composites for enhanced high voltage performance in Li ion batteries. *J. Electrochem. Soc.* **160,** A832–A837 (2013).
22. Fang, X., Ge, M., Rong, J. & Zhou, C. Graphene-oxide-coated LiNi$_{0.5}$Mn$_{1.5}$O$_4$ as high voltage cathode for lithium ion batteries with high energy density and long cycle life, *J. Mater. Chem. A* **1,** 4083–4088 (2013).
23. Wang, L., Li, H., Huang, X. & Baudrin, E. A comparative study of Fd-3m and P4$_3$32 "LiNi$_{0.5}$Mn$_{1.5}$O$_4$". *Solid State Ionics* **193,** 32–38 (2011).
24. Oh, S. H. *et al.* Structural and electrochemical investigations on the LiNi$_{0.5-x}$Mn$_{1.5-y}$M$_{x+y}$O$_4$ (M = Cr, Al, Zr) compound for 5 V cathode material. *J. Alloys Comp.* **469,** 244–250 (2009).
25. Amdouni, N., Zaghib, K., Gendron, F., Mauger, A. & Julien, C. M. Structure and insertion properties of disordered and ordered LiNi$_{0.5}$Mn$_{1.5}$O$_4$ spinels prepared by wet chemistry. *Ionics* **12,** 117–126 (2006).
26. Wang, H., Xia, H., Lai, M. O. & Lu, L. Enhancements of rate capability and cyclic performance of spinel LiNi$_{0.5}$Mn$_{1.5}$O$_4$ by trace Ru-doping. *Electrochem. Commun.* **11,** 1539–1542 (2009).
27. Kunduraci, M. & Amatucci, G. G. Effect of oxygen non-stoichiometry and temperature on cation ordering in LiMn$_{2-x}$Ni$_x$O$_4$ (0.50 > x > 0.36) spinels. *J. Power Sources* **165,** 359–367 (2007).
28. Xia, H., Tang, S. B., Lu, L., Meng, Y. S. & Ceder, G. The influence of preparation conditions on electrochemical properties of LiNi$_{0.5}$Mn$_{1.5}$O$_4$ thin film electrodes by PLD. *Electrochim. Acta* **52,** 2822–2828 (2007).
29. Van der Ven, A., Marianetti, C., Morgan, D. & Ceder, G. Phase transformations and volume changes in spinel Li$_x$Mn$_2$O$_4$. *Solid State Ionics* **135,** 21–32 (2000).
30. Xia, H., Meng, Y. S., Lu, L. & Ceder, G. Electrochemical properties of nonstoichiometric LiNi$_{0.5}$Mn$_{1.5}$O$_{4-\delta}$ thin-film electrodes prepared by pulsed laser deposition. *J. Electrochem. Soc.* **154,** A737–A743 (2007).
31. Arun, N. *et al.* Exceptional performance of a high voltage spinel LiNi$_{0.5}$Mn$_{1.5}$O$_4$ cathode in all one dimensional architectures with an anatase TiO$_2$ anode by electrospinning. *Nanoscale* **6,** 8926–8934 (2014).
32. Xiao, J. *et al.* High-performance LiNi$_{0.5}$Mn$_{1.5}$O$_4$ spinel controlled by Mn^{3+} concentration and site disorder. *Adv. Mater.* **24,** 2109–2116 (2012).
33. Wang, G., Xie, J., Zhu, T., Zhao, X. & Zhang, S. Self-templating synthesis of single crystalline LiNi$_{0.5}$Mn$_{1.5}$O$_4$ nanotubes with improved electrochemical performance. *Funct. Mater. Lett.* **7,** 1450009 (2014).
34. Qian, Y., Fu, Y., Wang, X. & Xia, H. LiNi$_{0.5}$Mn$_{1.5}$O$_4$ nanorod clusters as cathode material for high energy and high power lithium-ion batteries. *J. Nanosci. Nanotech.* **14,** 7038–7044 (2014).
35. Jan, S. S., Nurgul, S., Shi, X. Q., Xia, H. & Pang, H. Improvement of electrochemical performance of LiNi$_{0.8}$Co$_{0.1}$Mn$_{0.1}$O$_2$ cathode material by graphene nanosheets modification, *Electrochim. Acta* **149,** 86–93 (2014).

Acknowledgments

Author Contributions

H.X., X.T. and S.S. designed project, carried out data analyses and co-wrote the manuscript. Y.Q. and J.N. performed the materials characterization. S.S. and S.A. also contributed equally to the discussion presented in this paper.

Additional Information

Supplementary information accompanies this paper at http://www.nature.com/srep

Competing financial interests: The authors declare no competing financial interests.

How to cite this article: Tang, X. *et al.* Graphene wrapped ordered LiNi$_{0.5}$Mn$_{1.5}$O$_4$ nanorods as promising cathode material for lithium-ion batteries. *Sci. Rep.* **5,** 11958; doi: 10.1038/srep11958 (2015).